

Unequal mass binary neutron star mergers and multimessenger signals

Luis Lehner,¹ Steven L. Liebling,² Carlos Palenzuela,³ O. L. Caballero,⁴ Evan O'Connor,⁵ Matthew Anderson,⁶ and David Neilsen⁷

¹*Perimeter Institute for Theoretical Physics, Waterloo, Ontario N2L 2Y5, Canada*

²*Department of Physics, Long Island University, Brookville, New York 11548, USA*

³*Departament de Física, Universitat de les Illes Balears and Institut*

d'Estudis Espacials e Catalunya, Palma de Mallorca, Balears E-07122, Spain

⁴*Department of Physics, University of Guelph, Guelph, Ontario N1G 2W1, Canada*

⁵*Department of Physics, North Carolina State University, Raleigh, North Carolina 27695, USA*

⁶*Pervasive Technology Institute, Indiana University, Bloomington, IN 47405, USA*

⁷*Department of Physics and Astronomy, Brigham Young University, Provo, Utah 84602, USA*

(Dated: March 3, 2016)

We study the merger of binary neutron stars with different mass ratios adopting three different realistic, microphysical nuclear equations of state, as well as incorporating neutrino cooling effects. In particular, we concentrate on the influence of the equation of state on the gravitational wave signature and also on its role, in combination with neutrino cooling, in determining the properties of the resulting hypermassive neutron star, of the neutrinos produced, and of the ejected material. The ejecta we find are consistent with other recent studies that find that small mass ratios produce more ejecta than equal mass cases (up to some limit) and this ejecta is more neutron rich. This trend indicates the importance with future kilonovae observations of measuring the individual masses of an associated binary neutron star system, presumably from concurrent gravitational wave observations, in order to be able to extract information about the nuclear equation of state.

Contents

I. Introduction	1
II. Numerical Implementation	2
III. Results	2
A. Gravitational Waves	2
B. Matter dynamics: Outflow and Ejecta	6
C. Neutrino Emission	9
IV. Conclusions	12
Acknowledgments	13
References	13

I. INTRODUCTION

The spectacular detection of gravitational waves in event GW150914 [1] marks the start of the gravitational wave astronomy era. While this *first direct detection* corresponds to a signal produced by the merger of a binary black hole system, the existence of gravitational waves and our ability to detect them have been dramatically demonstrated. This observation will surely intensify efforts to identify potential signals in the various bands (gravitational wave, electromagnetic wave, and even neutrinos for sufficiently close events). An early example of this tantalizing possibility is the possible—and puzzling—connection of GW150914 with an observation by Fermi Gamma-ray Burst Monitor (GBM) [2] (see however [3, 4]). This new era of multimessenger astron-

omy will not only help test gravity and unravel spectacular astrophysics events but, importantly, enhance the detection possibilities themselves. The flurry of activity prompted by GW150914 serves as a clear example of what this era will bring. For instance, just to name a few examples, this single GW observation has spurred efforts to: test the basic tenants of General Relativity (e.g. [5–7]), infer astrophysical consequences on binary black hole population (e.g. [8, 9]), discuss possible mechanisms to explain the rather large stellar masses extracted from the signal (e.g. [10, 11]), and re-examine how to possibly channel electromagnetic counterparts in stellar mass binary black holes (e.g. [12, 13]).

Among compact binary systems, binary neutron star systems present very exciting prospects both in terms of providing strong signals and for the underlying physics able to be explored. For example, tidal effects during the late orbiting stages are imprinted on the gravitational wave signal and the interaction of the stars with their surrounding plasma can power pulsar-like electromagnetic signals from radio to gamma ray wavelengths [14–16]. The merger of such a system produces a differentially rotating, hot massive neutron star (MNS) with a strong neutrino luminosity. Depending on the masses involved and the EOS describing the stars, this massive remnant may collapse to a black hole, allowing for signals to reveal the “birth cry” of a black hole [17]. Such a black hole could lead to hyper-accretion and a short gamma-ray burst (sGRB) or related phenomena. The merger itself could produce significant outflow such that the ejected material might power a kilonova. A first reported of kilonova observation has been presented in [18, 19]. Furthermore, binary neutron star systems are important to test for alternative theories of gravity describing dynam-

ics that depart significantly from the expected one in General Relativity, even when binary black holes behave precisely as in GR [20–22]. Interestingly, such departures might be difficult to extract solely via gravitational waves [23] and complementary electromagnetic information will be important for such a task [24].

The dynamics and identification of potential signals of such a complicated system are complex, generally requiring numerical simulation of dynamical gravity, magnetized plasma, matter described with a realistic EoS, and finally the ability to track the dominant nuclear reactions involving neutrinos. Here we present the results of our latest studies of the merger of systems of two, unequal mass, neutron stars.

Our results suggest that unequal mass binaries, relative to the equal mass case, produce more ejecta that is cool and neutron rich because the ejecta has been tidally ripped from the constituent stars. That this material is neutron rich provides a likely environment for r-process nucleosynthesis and may produce an afterglow consistent with a kilonova. Additionally, a radio counterpart might be produced as this material interacts with the interstellar medium surrounding the binary. We provide estimates of the strength and time scales for such counterparts. Contrary to the equal mass case, we note that essentially all unequal mass cases studied produce enough ejecta that is sufficiently neutron rich for a related kilonova to peak in the infrared. This indicates that individual mass estimates through gravitational wave information may be crucial to extract EoS information using kilonovae observations from generic binary neutron star mergers. We illustrate difficulties in obtaining EoS information just from gravitational waveforms based on a small number of events unless post-merger detection and analysis is within reach. In such a case, if prompt collapse to black hole does not take place, extraction of the dominant gravitational wave mode produced by the remnant can provide a clean connection with the neutron star equation of state, and we present a simple fit connecting the (possibly) observable frequency with the star’s characteristics. In addition, we estimate neutrino luminosities and their dependence on EoS and mass ratio and discuss possible features that can potentially provide complementary information on the EoS. We summarize details in section II, present results in section III, and discuss these results in section IV.

II. NUMERICAL IMPLEMENTATION

The evolution equations for the spacetime and the fluid are already described in our previous paper [25], while full details of our implementation are described in [26]. Unless otherwise specified, we adopt geometrized units where $G = c = M_\odot = 1$, except for some particular results which are reported more naturally in physical cgs units.

Our stars consist of a fluid described by the stress en-

ergy tensor

$$T_{ab} = hu_a u_b + P g_{ab}, \quad (1)$$

where h is the fluid’s *total* enthalpy $h \equiv \rho(1 + \epsilon) + P$, and $\{\rho, \epsilon, Y_e, u^a, P\}$ are the rest mass energy density, specific internal energy, electron fraction (describing the relative abundance of electrons compared to the total number of baryons), four-velocity, and pressure of the fluid, respectively.

To track the composition of the fluid and the emission of neutrinos we employ a leakage scheme. In particular, the equations of motion consist of the following conservation laws

$$\nabla_a T_b^a = \mathcal{G}_b, \quad (2)$$

$$\nabla^a (T_{ab} n^b) = 0, \quad (3)$$

$$\nabla_a (Y_e \rho u^a) = \rho R_Y, \quad (4)$$

The sources \mathcal{G}_a ($\equiv -\nabla_c \mathcal{R}_a^c$) and R_Y correspond to the radiation four-force density and lepton sources and are computed within the leakage scheme. These equations are conservation laws for the stress-energy tensor, matter, and lepton number, respectively. Notice that, in the absence of lepton source terms ($R_Y = 0$), Eq. (4) provides a conservation law for leptons, and is similar to the familiar baryon conservation law, i.e., Y_e is a mass scalar.

III. RESULTS

We extend our previous work [25] and study the merger of *unequal mass neutron star binaries*. In particular, we concentrate on systems with parameters consistent with current observations (see e.g. [27]). Therefore, we will consider binaries with the same total gravitational mass $M = 2.70M_\odot$ and with different mass ratios $q \equiv M_1/M_2$ between 1 (the equal mass case) and 0.76

We continue with the same three distinct microphysical EoS (SFHo [28], DD2 [29] and NL3 [29]) used in our previous paper [25]. These three EoS were chosen to span a range of stiffnesses and they produce cold neutron stars with radii ranging from ≈ 12 km with the SFHo soft EoS to ≈ 15 km with the NL3 stiff EoS (for the same mass of $1.35M_\odot$). All three EoS are consistent with neutron stars having a mass of at least $2M_\odot$, and they are therefore consistent with observations of NS masses [30, 31].

We focus here on the late stages of the coalescence, comprising the last 4–6 orbits (depending on EoS), of irrotational binary neutron star systems. The physical parameters of the binaries and our grid setup are summarized in Table I.

A. Gravitational Waves

Before describing the characteristics of the GW signals, consider first the 2-body, Post-Newtonian approximation for a compact binary system (as can be found

EoS	q	ν	$m_b^{(1)}, m_g^{(1)}$ [M_\odot]	$m_b^{(2)}, m_g^{(2)}$ [M_\odot]	$R^{(1)}$ [km]	$R^{(2)}$ [km]	$C^{(1)}$	$C^{(2)}$	J_0^{ADM} [$G M_\odot^2/c$]	Ω_0 [rad/s]	f_0^{GW} [Hz]	M_{eject} [$10^{-3} M_\odot$]
NL3	1.0	0.250	1.47, 1.36	1.47, 1.36	14.80	14.80	0.136	0.136	7.40	1778	566	0.015
NL3	0.85	0.248	1.34, 1.25	1.60, 1.47	14.75	14.8	0.125	0.147	7.35	1777	566	2.3
DD2	1.0	0.250	1.49, 1.36	1.49, 1.36	13.22	13.22	0.152	0.152	7.39	1776	565	0.43
DD2	0.85	0.248	1.36, 1.29	1.62, 1.47	13.20	13.25	0.144	0.164	7.34	1775	565	0.42
DD2	0.76	0.245	1.27, 1.18	1.71, 1.54	13.16	13.25	0.132	0.172	7.26	1775	565	1.3
SFHo	1.0	0.250	1.50, 1.36	1.50, 1.36	11.90	11.90	0.169	0.169	7.38	1775	565	3.4
SFHo	0.85	0.248	1.37, 1.25	1.63, 1.47	11.95	11.85	0.154	0.183	7.31	1773	564	2.2

TABLE I: Summary of the binary neutron star systems considered in this work. The initial data were computed using the BIN STAR solver from the LORENE package [32], with the assumption that the stars have an initial constant temperature of $T = 0.02$ MeV and are in beta-equilibrium. All the binaries have a total mass $M_0^{\text{ADM}} = 2.7M_\odot$ and start from an initial separation of 45 km. The outer boundary is located at 750 km and the highest resolution covering both stars is $\Delta x_{\text{min}} = 230m$. The table displays the mass ratio of the binary $q \equiv M_1/M_2$ and $\nu = M_1 M_2 / M^2 = q/(q+1)^2$, the baryon (gravitational) mass of each star $m_b^{(i)}$ ($m_g^{(i)}$), its circumferential radius $R^{(i)}$ and its compactness $C^{(i)}$ (i.e., when the stars are at infinite separation), the angular momentum J_0^{ADM} , the initial orbital angular frequency Ω_0 , the initial GW frequency $f_0^{\text{GW}} \equiv \Omega_0/\pi$ of the system, and finally the total mass ejected during the merger process, M_{eject} .

in, for example, Ref. [33]). This approximation describes the interaction via an expansion with respect to the parameter $x \equiv (M\omega)^{2/3}$ where M is the total mass and ω is the orbital frequency. At the lowest order, $x = M/R$ with R the separation of the binary.

The amplitude of the gravitational waves produced, h (and consequently the energy radiated and angular momentum loss), from the system are, to leading order, given by the scaling $h \propto \mathcal{M}^{5/3} \omega^{2/3} / r$. Here the chirp-mass is defined as $\mathcal{M} \equiv (m_1 m_2)^{3/5} / (m_1 + m_2)^{1/5}$ and r is the distance to the source. Higher order contributions containing both conservative and dissipative pieces, depending on the constituent masses, spin, radiation-reaction, and internal structure, become increasingly important as the frequency (separation) increases (decreases) (see e.g. [33]).

Particularly relevant for our current discussion are tidal effects and the effect of mass ratio. For the former, given a mass ratio [87] $q \equiv m_1/m_2$, the chirp mass is $\mathcal{M} = M q^{3/5} / (1+q)^{6/5}$ [which is also $= 2^{-6/5} M (1 - 3\delta^2/20 + \mathcal{O}(\delta^3))$ in terms of $\delta \equiv 1 - q$]. Thus the dominant contribution to the gravitational wave amplitude is already sensitive to the mass ratio.

However, for realistic binary neutron star systems, the parameter q is limited to a small range and $3\delta^2/20 \simeq \{0, 3 \times 10^{-3}, 9 \times 10^{-3}\}$ for $q = \{1, 0.85, 0.76\}$ thus mass ratio differences in BNS systems are small.

Tidal effects, on the other hand, can become quite significant at close separations, appearing with a high power of the inverse of the stellar compactness. In particular, even though tidal effects enter the PN approximation at tenth order in x , this sub-leading effect can still be apparent at sufficiently high frequencies since $C_i \in (0.05 - 0.2)$ for neutron stars. That is, the leading contribution to the tidal force on a single star is given by

$$F_T \propto k_2^{(i)} C_i^{-5} x^{10} \quad (5)$$

where $k_2^{(i)}$ is the quadrupolar tidal coupling Love num-

ber constant and $C_i = M_i/R_i$ (for the i th star) [34, 35]. The dependence of tidal effects on the binary's dynamics can be expressed via κ_2^T for the binary in terms of the individual $k_2^{(i)}$, defined as [36, 37]

$$\kappa_2^T = 2 \left[\frac{q^4}{(1+q)^5} \frac{k_2^{(1)}}{C_1^5} + \frac{q}{(1+q)^5} \frac{k_2^{(2)}}{C_2^5} \right]. \quad (6)$$

For neutron stars, the Love number constant typically $\in (10^{-2}, 0.5)$ [38] and their compactness ratios $C \simeq 0.1 - 0.2$. Thus for sufficiently high frequencies (close separations) tidal effects can become important as $\kappa_2^T x^{10} \simeq \mathcal{O}(1)$. Notice that for a fixed given total mass, stiffer EoS (i.e., with larger radii and smaller compactness) lead to larger κ_2^T and therefore stronger tidal effects. Similarly, unequal mass cases also lead to slightly larger κ_2^T thus enhancing tidal effects. For low frequencies on the other hand, $\kappa_2^T x^{10} \ll \mathcal{O}(1)$, and only the mass ratio can introduce departures when comparing binaries with the same total mass. However, these departures are necessarily small for BNS systems.

The consequences of the above observations are clearly illustrated in Figs. 1 and 2. Fig. 1 shows the (coordinate) separation versus time for all EoS and mass ratios studied while Fig. 2 displays the gravitational wave signals as computed by the Newman-Penrose scalar Ψ_4 .

The times in Fig. 2 have been relabeled in terms of a merger time. For each EoS, all mass ratios use the same time. In particular, the merger time is the time at which, for the $q = 1$ case, the two locations of density maxima (the centers of the two stars) decreases below a threshold distance (generally the sum of the two stellar radii), corresponding to the stars making contact. Because the signals in each panel of Fig. 2 share the same time, we have included a vertical line to denote the time when such contact occurs for the unequal mass cases. As can be clearly appreciated in both figures, the early behavior of all mass ratios within a given EoS (< 7 ms) agree.

However, as the orbit tightens tidal deformations increase and affect the dynamics of the system. Their effects manifest first for binaries described by the NL3, followed by the DD2, and finally the SFHo equations of state. As expected from our discussion above, this succession is tied to the decreasing radii characterizing the stars of each binary. For instance, Fig. 1 indicates that a more rapid plunge takes place for stars with larger radii, and, interestingly, within the same EoS the merger takes place earlier as the mass ratio is decreased. This behavior is apparent in the gravitational wave signatures in which binaries with large stellar radii demonstrate differences earlier than those binaries with smaller radii. Furthermore, comparison within the same EoS reveals that, as the mass ratio decreases, an earlier departure from a simpler (chirping) sinusoidal wave arises as tidal effects become more important. This pre-merger behavior is especially clear for the NL3 case but is essentially negligible for the softer EoS considered.

Additionally $q \neq 1$ cases also display a stronger $l = 2, m = 1$ component in the gravitational waves during the late pre-merger and afterwards than the $q = 1$ case. However, such modes are still at least a couple of orders of magnitude weaker than the main $l = 2, m = 2$ signal displayed in Fig. 2. Nevertheless, they can strongly seed a possible $m = 1$ instability after the merger whose associated frequency would be lower than the one corresponding to $m = 2$ modes [39, 40].

The post-merger behavior is governed by the properties of the resulting hot, differentially rotating MNS (or hypermassive NS) which loses energy and angular momentum via emission of neutrinos and gravitational waves. Depending on the EoS and the total mass, the remnant MNS may eventually collapse to a black hole or continue as a rotating star. In cases that avoid prompt collapse to a black hole [88], gravitational waves in this stage are characterized by a few dominant modes with frequencies intimately tied to the EoS. These dominant modes arise are determined by the natural oscillation frequencies of the star, by the details of the merger process itself, and by the possible development of an $m = 1$ instability if a rather long-lived MNS is possible. Naturally, these modes are a potentially rich source of information about the system (see for instance [41] and references within).

We scrutinize these modes more closely by computing the Fourier transform of the primary Ψ_4 gravitational wave mode ($l = 2 = m$) in a time window of duration roughly 10 ms after the merger. These spectra, shown in Fig. 3, demonstrate several characteristic peaks, and these peak frequencies are presented in Table II. The most dominant of these modes, using the terminology of Ref. [42], f_{peak} , is associated with the rotational behavior and quadrupolar structure of the newly formed MNS/HMNS. Secondary modes, at lower frequencies, can be associated with different mechanisms [39, 42–44]. However as noted in [42], in low total mass binaries [45] and for the case of a stiff EoS as in Ref. [46], (the majority of) these secondary modes degrade quickly with

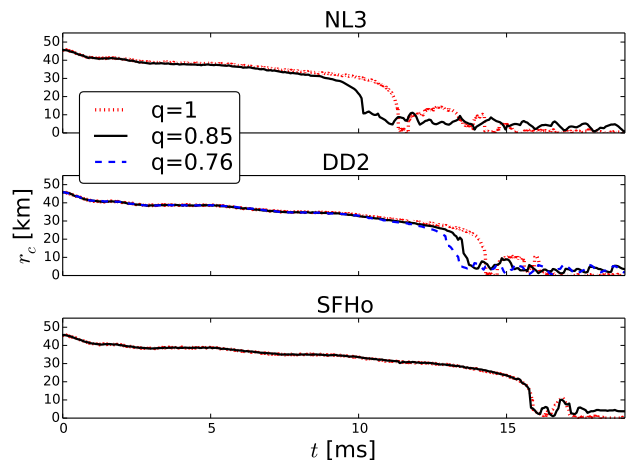


FIG. 1: The coordinate separation between the centers of the stars as a function of time for different mass ratios and EoS. Overall, unequal mass binaries merge more quickly than equal mass binaries, and the time to merger increases for softer equations of state with smaller stellar radii. The coordinate distance is approximated by the positions of the maximum densities.

time in just a few milliseconds and are unlikely to build enough SNR for detection. The primary mode on the other hand, can last for long times and provide the best opportunity for detection. Consequently it has been the focus of increased scrutiny.

Recently, a fit for these modes has been suggested for the case of equal mass binaries [42], and we include in Table II the frequencies predicted from this fit together with our measured values. As discussed in our previous work [25], our results for $q = 1$ are within 10% of the predicted frequencies.

A similar fit for unequal mass binaries described by tabulated EoS is so far unavailable because, contrary to the equal mass case, studies with $q \neq 1$ are still in their infancy. The majority of currently available results for unequal mass binaries employ piece-wise polytropes (chosen to be reasonable approximations to tabulated, realistic EoS.). A comparison of results obtained with the so-called MS1, H4, SLy cases, studied in [47], which have similar mass ratios and masses to those used here for the NL3, DD2, SFHo EoS, reveals that the peak frequencies agree to better than 5%. As well, Ref. [46] found that, for the polytrope dubbed SLyPP (which yields a NS similar to the one described by the NL3 EoS considered here), the resulting peak frequency, f_{peak} , has a small dependence on the mass ratio, with a slightly higher frequency for the equal mass case. This finding is also consistent with our results. Last, relatively small differences in the peak frequency with respect to mass ratio have also been reported in other recent works [37, 42, 48]. As can be appreciated in Table II, we also find that the peak frequencies for $q \neq 1$ lie within $\approx 10\%$ of the corresponding $q = 1$ case and are typically lower —except for $q = 0.85$

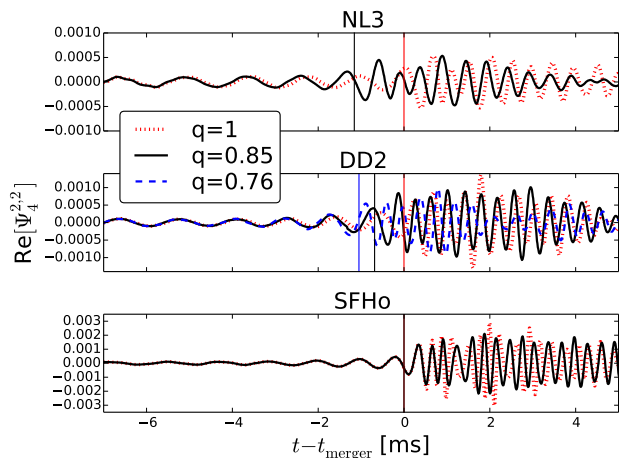


FIG. 2: A comparison of the gravitational wave signals near merger using the primary mode of Ψ_4 . The signals have been shifted in time such that $t = 0$ corresponds to the moment of contact for $q = 1$, with respect to each EoS, and vertical bars indicate the moment of contact for the other cases [the time labels are the same in all panels]. For NL3 and to a lesser extent for DD2, clear differences in the waveforms arise prior to the stars coming into contact. In contrast, the SFHo waveforms show essentially no differences before merger. After the merger however, there are significant differences between all of the waveforms, showing that they carry information about the post-merger star, e.g., internal structure, radius, compactness, etc., that is sensitive to the equation of state.

DD2.

Beyond comparing with particular fits, it is instructive to take a step back and consider estimating the peak frequency based on simple arguments which can shed light on the underlying physics of the system. A simple approach is to consider the contact frequencies, f_c , of the binary, based on the radii of the two stars. This approach can only provide a lower bound but it may potentially lead to improved estimates in the future. The contact frequency [89] is given in terms of the binary parameters by (in M^{-1} units)

$$f_c = \frac{1}{\pi M_g} \left(\frac{m_g^{(1)}}{M_g C_1} + \frac{m_g^{(2)}}{M_g C_2} \right)^{-3/2} \quad (7)$$

where $M_g = m_g^{(1)} + m_g^{(2)}$, (see Eq. (36) of Ref. [49]). We include with our measured frequencies the estimated contact frequencies in Table II. While they are clearly lower than the observed frequencies as anticipated, they do provide a consistent trend.

This trend is more clearly seen in Fig.4 which illustrates the measured peak frequency versus the estimated contact frequency for all cases studied here (which corresponds to total mass $M = 2.7M_\odot$) together with data from Ref. [42] (for equal mass binaries with $M = 2.4M_\odot$). The observed trend can be expressed quantita-

EoS	q	f_1	f_2	f_3	f_4	f_{peak}	f_{spiral}	f_{2-0}	f_c
NL3	1.0	2.03	1.54	0.83	—	2.2	1.6	1.2	1.19
NL3	0.85	2.01	1.61	1.37	0.8	—	—	—	1.19
DD2	1.0	2.34	1.97	1.82	1.62	2.6	1.9	1.5	1.41
DD2	0.85	2.58	1.92	1.62	—	—	—	—	1.42
DD2	0.76	2.32	1.86	1.62	—	—	—	—	1.41
SFHo	1.0	3.45	2.59	2.20	1.62	3.2	2.4	2.1	1.65
SFHo	0.85	3.29	2.29	1.61	—	—	—	—	1.65

TABLE II: Prominent oscillation frequencies (kHz) in the power spectral densities of the post-merger gravitational waveform compared with predicted values. The frequencies f_1 , f_2 , f_3 , and f_4 correspond to various peaks of the post-merger GW spectrum (see Fig. 3). f_{peak} and f_{spiral} are the predicted peak frequencies from Ref [42]. The correspondence between f_1 and f_{peak} , f_2 and f_{spiral} , and either f_3 or f_4 with f_{2-0} suggests consistency with the model presented in [42] (which was tailored for the equal mass case, but reports errors $< 5\%$ for mass ratios $q = 0.92$). f_c is the computed contact frequency 7.

tively through a linear regression fit to our data

$$f_{\text{peak}}[\text{kHz}] = -1.61 + 2.96 f_c \left[\frac{2.7M_\odot}{M} \right] [\text{kHz}]. \quad (8)$$

This correlation is characterized by a correlation coefficient = 0.96 and has been obtained with total mass $M = 2.7M_\odot$. For systems with a different total mass, Eq. (8) effectively rescales the contact frequency.

For instance, Ref. [45] presented peak frequencies from evolutions of equal mass binaries with total mass $M = 2.4M_\odot$ concentrating on three EoS: the same DD2 and SFHo EoS studied here along with LS220 [50] which yields radii in between the other two for the same mass. The corresponding peak frequencies computed for DD2, LS220, and SFHo EoS are 2.35 kHz, 2.56 kHz, and 2.96 kHz, respectively. Expression (8) estimates the peak frequencies to be $f_{\text{peak}} = 2.32$ kHz, 2.49 kHz, and 2.91 kHz, respectively, for these cases. The agreement is quite good. It would be interesting to explore if this simple approach works as well in the case of spinning binaries (e.g. [39, 51]) and to contrast it to alternative fits depending explicitly on tidal deformability parameters [52].

Finally, beyond the specific dynamics and waveform characteristics, it is instructive to explore the extent to which the obtained waveforms could be distinguished with respect to different configurations of aLIGO. To do so, we first obtain a longer wavetrain by employing at earlier times a PN (Taylor T4) expansion augmented to include leading order tidal effects as described in Refs. [34, 53]. We match this augmented PN signal at early times to our numerical signal before merger to form a hybrid waveform. (Further improvements in the early signal can be achieved, see e.g. [52, 54], though such improvements would not affect the main conclusions drawn here.) The matching is accomplished by choosing a cycle devoid of the initial numerical transients but still well be-

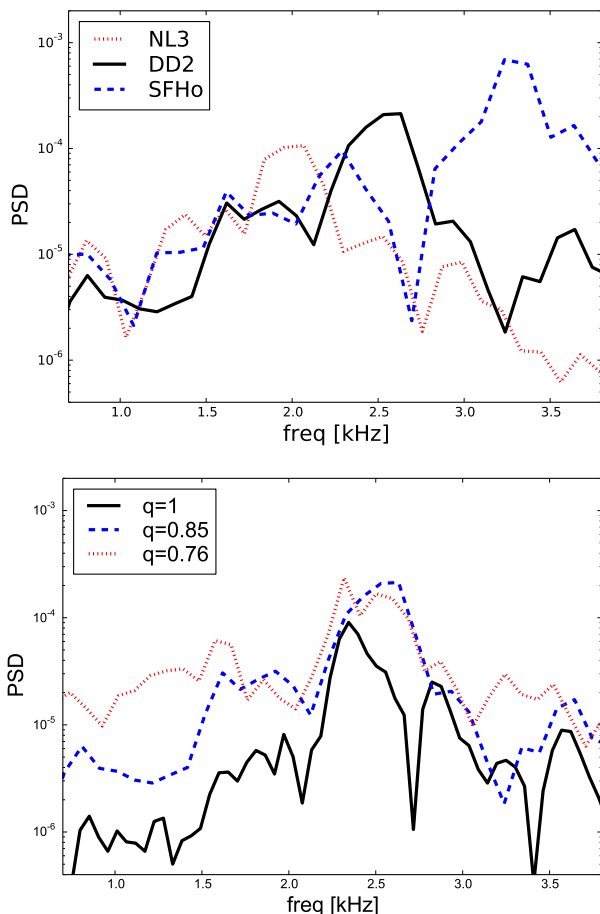


FIG. 3: Power spectral densities (PSD) of the gravitational waveforms after the BNS merger for the three different equations of state. The peaks in the Fourier transform of the waveforms represent the dominant oscillation modes of the MNS, f_i , presented in Table II. (Top:) The PSDs for the $q = 0.85$ cases with the three different EoS. (Bottom:) The PSDs for three values of q for just the DD2 EoS.

fore merger. Within this cycle, a weighted average of the two waveforms is calculated using a tanh function that transitions from 0 to 1.

Fig. 5 illustrates the strain of the waveforms for the different cases considered here with respect to two possible noise curves from aLIGO for binaries at 100 Mpc. As can be appreciated in the figure, essentially no differences exist that could be discerned with the “No SRM” noise curve *with a single event at such a distance*. The more aggressive noise curve corresponding to the “Zero Detuned, High Power” configuration would, however, be sensitive to differences between the stiffest and softest EoS considered.

As a figure of merit, it is instructive to contrast the distinguishability of the obtained waveforms. Since we start all our simulations at the same separation (orbital frequency) we compute the “distinguishability” between the different waveforms (as described in e.g. [55], see also [56–

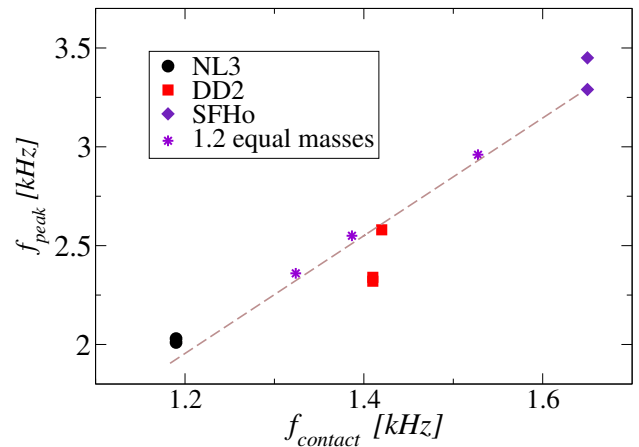


FIG. 4: After-merger peak-frequency computed via simulations versus the estimated contact frequency for several BNS mergers. In addition to the quantities calculated in this paper, we include results for an equal-mass binary neutron star system with a smaller total mass from Ref. [45], which used the DD2, LS220, and SFHo equations of state.

EoS	DD2, q085	SFHo, q085	NL3, q085
DD2, q076	1.70 (0.09)	1.078 (0.05)	1.50 (0.07)
DD2, q085		0.96 (0.05)	0.77 (0.03)
SFHo, q085			0.77 (0.03)

TABLE III: The distinguishability between gravitational waveforms for binary mergers with different equations of state for the zero-detuned high power (no signal-recycling mirror) noise curves for aLIGO.

58]) using the “Zero Detuned, High Power” and the “No SRM” noise curves in aLIGO [59]. Table III lists the values obtained for $\delta h \equiv \sqrt{(h_i - h_j, h_i - h_j)}$ (without allowing for frequency shifts and without normalizing our waveforms). Values above 1 imply such waveforms could be distinguished, indicating therefore that DD2 waveforms for $q = 0.76$ could be distinguished from all the others when using the more aggressive noise curve. The other cases are not discernible, even when using the *Zero Detuned, High Power* noise curve.

The delicate nature of distinguishing EoS effects in binary neutron star systems has been thoroughly discussed in Refs. [60, 61], which stressed the need for tens of events to disentangling EoS differences if employing gravitational waves alone. Importantly, as discussed in, e.g. [25, 62–66] and later in this work, complementary electromagnetic information can help reveal the EoS from the characteristics of the radioactive decay of heavy elements produced by ejected material.

B. Matter dynamics: Outflow and Ejecta

The merger of a binary with the total mass considered here produces a hot, rotating neutron star that is

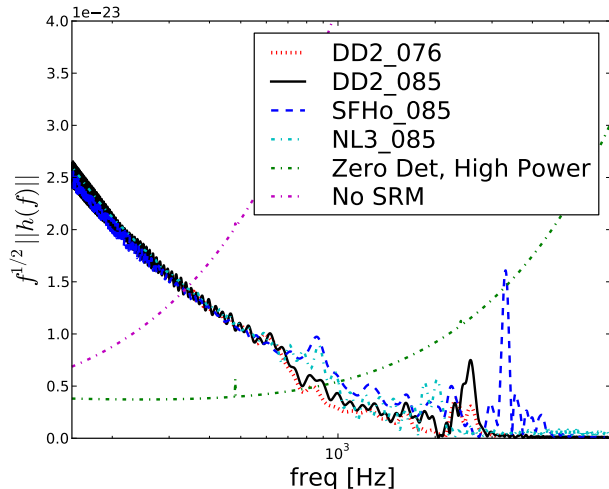


FIG. 5: The Fourier spectrum of the GW signals for the four binaries. The dotted and dashed-dotted monotonic curves at high frequencies show two fits to the noise power spectrum $\sqrt{S_h}$ of aLIGO (specifically the “zero-detuned high-power” and the “No Signal Recycling Mirror” (NSRM) cases [59]).

stable for some time against gravitational collapse to a black hole due to the rapid differential rotation and the thermal pressure. The merger that produces such a star is quite violent and, as a by product, a significant amount of material can be ejected from the binary. The characteristics of this ejecta is important as it can produce an associated electromagnetic signal [67–69] that can provide complementary information about the binary (e.g. [25, 45, 70, 71]).

The recent observation of an infrared transient associated with the SGRB 130603B [18, 19] has demonstrated that such a tantalizing prospect is within reach. Additionally as discussed in [72], bound matter might also induce observable electromagnetic signals through the properties of winds emitted by the system [72–74].

We thus concentrate here on describing the properties of outflow material and its dependence on both the nuclear EoS and the binary mass ratio. The latter is particularly relevant as this material generally originates via tidal effects and is therefore especially sensitive to the mass ratio. We analyze in detail the various binaries at ~ 3 ms after merger. A key distinction is made between matter remaining bound to the system and ejecta, i.e. material having kinetic energy sufficient to unbind it. Our analysis uses the common approach that material is considered unbound if its energy (defined by assuming that the spacetime is stationary) is positive.

We note that an important issue when studying low-density material in simulations adopting conservative “Eulerian” schemes (as opposed to Lagrangian schemes) is that the results in low density regions could be significantly affected by the artificial atmosphere employed

specifically to handle such regions. The simulations presented here benefit from an improvement to our code’s treatment of the atmosphere so that the floor value decreases rapidly with distance from the center of coordinates (similar to that used in [75]). Comparisons of the new atmosphere treatment with the original, as well as studies with different atmosphere values, indicates that the properties being presented are nearly-independent of this improvement when the atmosphere density is sufficiently small $\approx 5 \times 10^5 \text{ g/cm}^3 \approx 10^{-10} \rho_{\text{max}}$ and when estimates are calculated shortly after merger of $\leq 4 - 5$ ms.

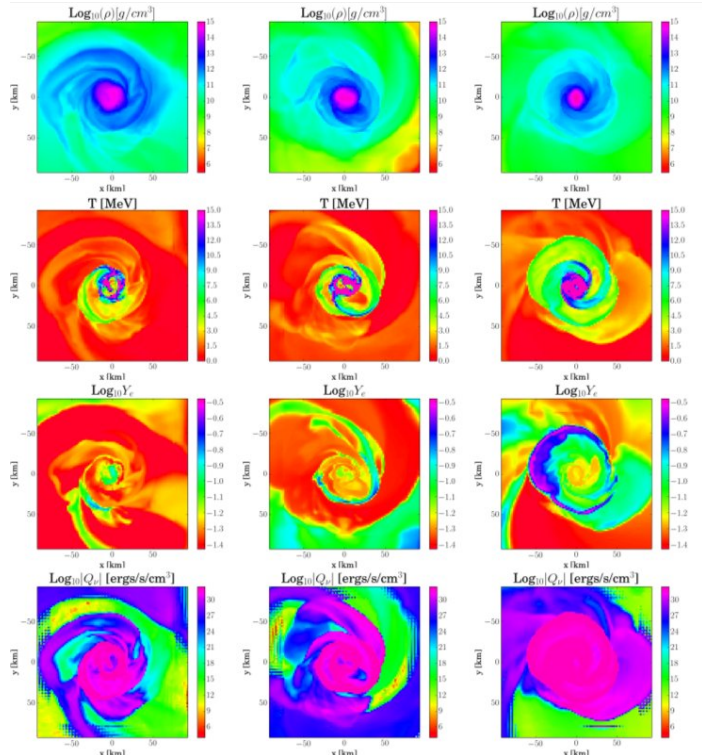


FIG. 6: Density, temperature, electron fraction, and neutrino luminosity rate for the different EoS on the $z = 0$ plane at roughly $t = 3$ ms after the merger. Shown are the NL3 EoS (left), DD2 EoS (middle), and SFHo (right) for the mass ratio $q = 0.85$.

We begin by considering all three EoS for the same mass ratio, $q = 0.85$. Fig. 6 displays various properties along the equatorial plane ($z = 0$), all roughly 3 milliseconds after merger. The density variations are similar to that seen in the equal mass case (see Figure 9 of [25]); the SFHo remnant is more centrally condensed compared to the remnants of the stiffer EoS that are less compact. Such behavior is expected as the collision takes place deeper in the gravitational potential of the system which, in turn, implies the remnant of the SFHo case is hotter than the other two. Also, while all three snapshots with different EoS show wisps of electron rich material just outside the remnants, the SFHo has the most significant of such regions. This is due to the larger matter temperatures in the SFHo remnant that drives decompression

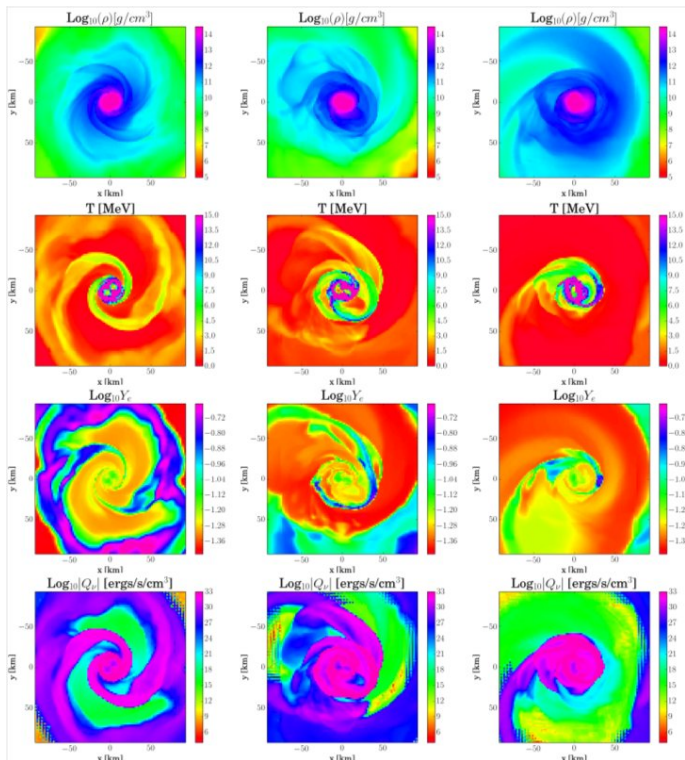


FIG. 7: Density, temperature, electron fraction, and neutrino luminosity rate for the DD2 EoS on the $z = 0$ plane at roughly $t = 3$ ms after the merger. Shown are the three mass ratios $q = 1$ (left), $q = 0.85$ (middle) and $q = 0.76$ (right).

of the hot material to lower densities where positron capture on neutrons can effectively raise the electron fraction. For all the EoS, there is evidence of tidal tails with one spiral arm stronger than the other. This asymmetry arises from the unequal mass ratio of the binary.

To more cleanly understand the role of mass ratio, we fix the EoS to that with the intermediate stiffness, DD2, and consider three mass ratios. Fig. 7 displays the same quantities as in Fig. 6 but instead for mass ratios $q = \{1, 0.85, 0.76\}$.

The density panels show that a decreased mass ratio results in a similar looking remnant but with more dispersed material outside it due to stronger tidal effects. The temperature looks roughly similar in the star, although slightly higher in the tidal tails of the equal mass cases. The electron fraction is noticeably lower in the decreased mass ratio simulations as is the neutrino emissivity. All the quantities display a strong spiral arm in the case of unequal masses, in contrast to the two spiral arms of the equal mass case. As we discuss later however, these broad properties do not convey what portion of this material is bound/unbound which is important in determining possible kilonova characteristics.

To this end, we integrate the characteristics of both the bound and the unbound matter and plot them as histograms (such calculations are described in Ref. [25]). In particular, we display the electron fraction in Fig. 8,

the temperature in Fig. 9, the velocity in Fig. 10 and the polar and azimuthal angles in Fig. 11. Using these histograms, we present some observations and follow these with a general discussion about these features.

Quite apparent in Fig. 8 is that bound material is generally quite neutron rich and independent of the mass ratio. However, the temperature distribution of this bound material does show some dependence on the mass ratio in Fig. 9. For the NL3 case, the dependence is minimal with the temperature distribution remaining generally the same among the mass ratios. The SFHo case shows the largest variation with mass ratio with the smaller mass ratio yielding a generally cooler merger remnant.

The ejecta, on the other hand, becomes increasingly neutron rich as the mass ratio departs from unity. Also apparent (in the insets) is that the amount of unbound material generally increases when the mass ratio decreases. We quantitatively summarize the amount of ejecta mass in Table I. The NL3 ejecta for the equal mass case is minuscule but significant for $q = 0.85$. The DD2 ejecta increases much less dramatically, but the SFHo breaks with this trend, albeit only moderately. The temperature of the ejecta is quite cool (< 5 MeV) for every EoS and mass ratio, as displayed in Fig. 9. The observed trend indicates that for lower values of q the ejected material is cooler, being dominated by neutron-rich, tidal tail material.

Another interesting observation comes from the angular distribution of the ejected material. Fig. 11 shows the azimuthal and polar angle distributions of unbound material. The histograms of polar angle do not show significant qualitative differences between the different mass ratio cases other than one observed trend. For low mass ratios the ejecta is more confined towards the equatorial region, giving quantitatively steeper distributions. The azimuthal distribution is more isotropic in the equal mass case (two spiral arms) but more anisotropic in the unequal mass cases (one spiral arm). As expected, the anisotropy grows as the mass ratio decreases from unity.

These observations suggest that a smaller mass ratio results in a less violent collision because the less massive star disrupts earlier and further out of the gravitational well than in the equal mass case. Only the NL3 bound material has essentially the same temperature for the different mass ratios. This EoS, however, has the largest stars generally, and so its equal mass case is already fairly cool. In contrast, the SFHo case has noticeably cooler bound and ejected material.

In general terms, the unbound matter (or ejecta) can be sourced either by tidal disruption during the merger or by thermal pressure and other interactions (e.g. shock heating) [On longer timescales –not studied here– an extra source is provided by winds or outflows from an accretion disk [73]]. Our work here concentrates mainly on the material produced by tidal interaction, and we observe that, as the mass ratio decreases, the tidal disruption occurs earlier and further out. Consequently, there is more tidal-ejecta mass for small mass ratios. Furthermore,

the temperature of this ejecta is lower, which inhibits positron production and capture on neutrons. Thus, the electron fraction is much closer to that of the original neutron star material. Only the SFHo retains essentially the same amount of ejected material with changes to the mass ratio because of a presumed balance of a competing effect; namely that the equal mass case was quite violent resulting in significant interaction ejecta (with higher values of Y_e and T) from shock heating. In the unequal mass case, the violence decreases (decreasing the interaction ejecta), but the early disruption increases the tidal ejecta. This explanation is consistent with the temperature and Y_e distributions of ejecta mass discussed above and shown in Figs. 8 and 9.

The current work is so far the only one of which we are aware studying unequal binaries employing realistic microphysical EoS; thus there is a lack of studies with which to compare, for instance, the amount of ejected material. As we did for the case of gravitational wave characteristics, we can compare our results to those obtained employing piecewise polytropic EoS. To do so we focus on cases studied using the so-called MS1, H4, SLy piece-wise polytropes from [37] which have similar mass ratios and masses to those used here for the NL3, DD2, SFHo EoS. The results are in reasonable agreement with some of the cases, with typical ejected masses of $10^{-4} - 10^{-3} M_\odot$ (although they find even $10^{-2} M_\odot$ for their softest EoS [SLy]). It is not clear if these differences come only from the EoS choice. Nevertheless the overall trend is the same, namely that *a*) softer EoS have larger ejecta and *b*) unequal mass cases, for a given EoS, have larger ejecta masses for stiff EoS (DD2 and NL3 in our case, MS1 and H4 in the case of [37]) and lower ejecta masses for soft EoS (SFHo in our case, SLy in [37]).

The ejecta values obtained here allow us to estimate the lag-times (with respect to merger) and luminosities corresponding to each case. An important property of ejecta with such a low value of Y_e is its ability to produce elements with high atomic mass number ($A \geq 120$) [76–78]. As argued in [79], due to the increased opacity as a result of lanthanides contributions, the expected emission from thermal decay of r-process elements would be dimmer/redder and delayed with respect to typical supernova expectations. Estimates in [79] (slightly re-arranged as in [39]) argue that the rise time of the corresponding kilonova emission t_{peak}^k (from the time of the merger) is given by

$$t_{\text{peak}}^k \approx 0.25 \text{ days} \left[\frac{M_{\text{eject}}}{10^{-2} M_\odot} \right]^{1/2} \left[\frac{v}{0.3c} \right]^{-1/2} \quad (9)$$

with a peak luminosity of

$$L \approx 2 \times 10^{41} \text{ erg/s} \left[\frac{M_{\text{eject}}}{10^{-2} M_\odot} \right]^{1/2} \left[\frac{v}{0.3c} \right]^{1/2}. \quad (10)$$

The values obtained for the cases studied are summarized in Table IV.

In addition to the electromagnetic signals produced by the decay of radioactive elements, another transient has been proposed as a result from the collision of the ejected material with the interstellar medium [80]. This interaction would produce a radio emission that evolves more slowly. Indeed, the estimated timescales and brightness are expected to obey [80] (employing the re-arranged version of [39])

$$t_{\text{peak}} \approx 6 \text{ yr} \left[\frac{E_{\text{kin}}}{10^{51} \text{ erg}} \right]^{1/3} \left[\frac{n_0}{0.1 \text{ cm}^{-3}} \right]^{-1/3} \left[\frac{v}{0.3c} \right]^{-5/3} \quad (11)$$

with a flux density

$$F(\nu_{\text{obs}}) \approx 0.6 \text{ mJy} \left[\frac{E_{\text{kin}}}{10^{51} \text{ erg}} \right] \left[\frac{n_0}{0.1 \text{ cm}^{-3}} \right]^{7/8} \left[\frac{v}{0.3c} \right]^{11/4} \left[\frac{\nu_{\text{obs}}}{1 \text{ GHz}} \right]^{-3/4} \left[\frac{d}{100 \text{ Mpc}} \right]^{-2}. \quad (12)$$

Table IV illustrates the values obtained for t_{peak} and $F(\nu_{\text{obs}})$ (for a representative value of $\nu_{\text{obs}} = 1 \text{ GHz}$) assuming a density of $n_0 = 0.1 \text{ cm}^{-3}$ and a distance of $d = 100 \text{ Mpc}$. The values of E_{kin} have been calculated for the unbound material as the total non-gravitational energy minus the rest mass and the internal energies [75].

C. Neutrino Emission

Finally we turn our attention to the neutrinos emitted by the system. We estimate the luminosity via a leakage scheme [81–83] and determine the thermodynamic properties of the neutrinospheres via a ray-tracing formalism [84]. The algorithms we employ to obtain both estimates have been described in our previous papers [26] and [25], respectively.

Figs. 6 and 7 illustrate both the spatial extent of the temperature and of the neutrino emissivities in the equatorial plane at $\sim 3 \text{ ms}$ after merger for the $q = 0.85$ mass ratio simulations across all EoS (NL3, DD2, SFHo), and for the DD2 EoS simulations across the three mass ratios considered ($q = 1.0, 0.85,$ and 0.76), respectively. The first figure indicates that softer EoS will give rise to higher neutrino luminosities which is consistent with observations in the equal mass case [25]. The higher luminosities are natural consequences of both the increased temperature and the increased amount of shock heating for the softer EoS. The higher temperatures also imply that the neutrino average energies will be higher.

These observations and conclusions are also supported by the results of our ray-tracing shown in Fig. 12. This figure shows the spatial distribution of the temperature of the electron neutrinosphere and electron antineutrinosphere for the $q = 0.85$ mass ratio simulations using three different EoS at $\sim 3 \text{ ms}$ after merger. They show higher peak matter temperatures at the electron (anti)neutrinosphere for the SFHo EoS, locally as high as $\sim 16 \text{ MeV}$ ($\sim 18 \text{ MeV}$), when compared to the NL3 EoS

EoS	q	$L[10^{40}\text{erg/s}]$	t_{peak}^k [days]	$M_{\text{eject}}[10^{-3}M_{\odot}]$	v/c	$E_{\text{kin}}[10^{50}\text{ergs}]$	t_{peak} [yr]	$F(1\text{ GHz})$ [mJy]
NL3	1.0	0.9	0.008	0.015	0.45	0.01	0.31	1.8×10^{-3}
NL3	0.85	8.8	0.13	2.3	0.25	1.22	4.0	4.4×10^{-2}
DD2	1.0	4.1	0.05	0.43	0.3	0.31	1.9	1.9×10^{-2}
DD2	0.85	4.1	0.05	0.42	0.3	0.29	1.8	1.7×10^{-2}
DD2	0.76	7.2	0.09	1.3	0.3	0.76	2.5	4.6×10^{-2}
SFHo	1.0	10.6	0.16	3.4	0.25	1.8	4.6	6.5×10^{-2}
SFHo	0.85	8.6	0.13	2.2	0.25	1.8	4.6	6.5×10^{-2}

TABLE IV: Estimated properties of electromagnetic (EM) signals after the merger. The rise-time t_{peak}^k and luminosity L of EM radiation from a potential kilonova are calculated from Eqs. (9) and (10). We used the middle value of the bin corresponding to the peak velocity (see Fig 10), v/c , in calculating these estimates. The lag time t_{peak} and flux density F , estimated from the collision of the ejecta with the interstellar medium, are calculated from Eqs. (11) and (12).

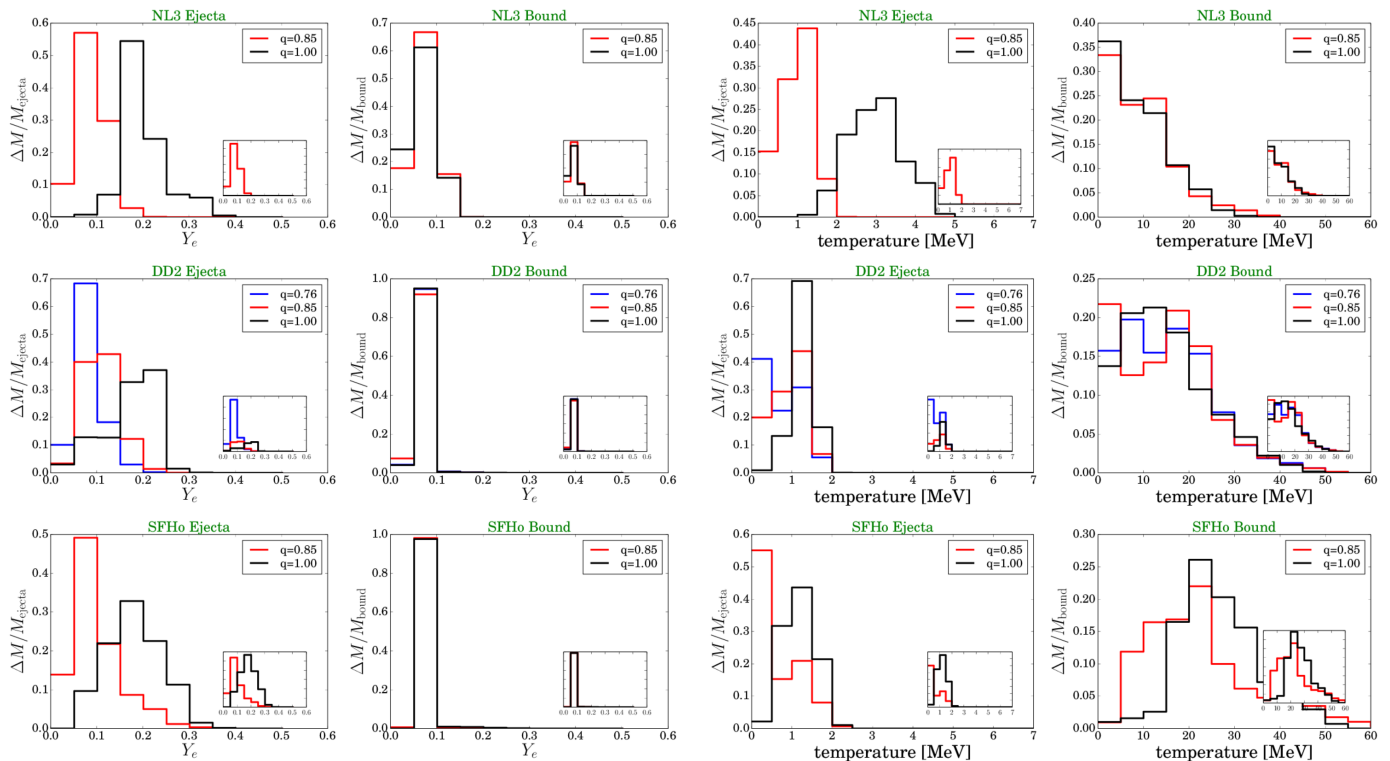


FIG. 8: *Distribution of the electron fraction for bound and unbound material.* The fractional quantity of material is displayed for the different bins, and in the insets the absolute quantities are shown. For all three EoS, the bound material hardly changes with the mass ratio. In contrast, the electron fraction generally decreases as the mass ratio decreases.

where the peak temperatures at the (anti)neutrinosphere reach ~ 12 MeV (~ 14 MeV). Our ray-tracing gives average electron neutrino (antineutrino) energies (as measured at infinity) for these same snapshots of ~ 12.6 MeV (~ 15.6 MeV), ~ 15.1 MeV (~ 18.1 MeV), and ~ 15.3 MeV (~ 17.8 MeV), for the NL3, DD2, and SFHo EoS, respectively. These average energies are also summarized in Table V.

We next consider the impact of the mass ratio on the

FIG. 9: *Temperature distribution of bound and unbound mass.* As in Fig. 8, the insets show the absolute quantities in arbitrary units. The ejecta is generally cold for any EoS and any mass ratio.

properties of the emitted neutrinos. Fig. 13 shows the neutrino surfaces ~ 3 ms after merger for the three mass ratios considered for the DD2 EoS. The maximum temperatures achieved at the neutrinospheres are ~ 14 MeV and correspond to the equal mass case. These maximum temperatures decrease to ~ 12 MeV for the smaller mass ratios. As q decreases, the matter distribution becomes more dispersed, a consequence of stronger tidal effects, and this effect is reflected in more dispersed neutrino surfaces that, in addition to reaching smaller maximum temperatures, display a more uniform temperature. This

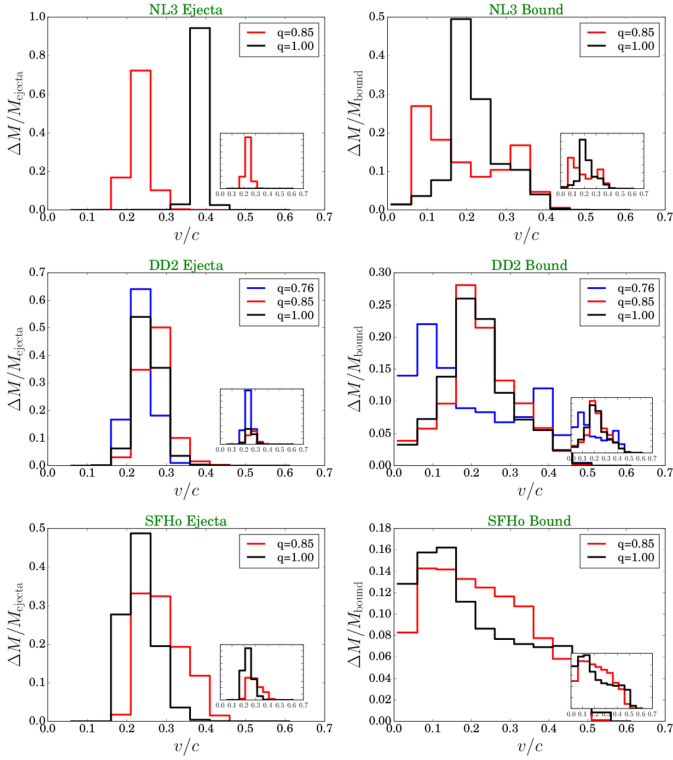


FIG. 10: *Velocity distribution of bound and unbound mass.* As in Figs. 8 and 9, the insets show the absolute quantities in arbitrary units.

more dispersed, but uniform, behavior can also be seen close to the core in the equatorial slices of Fig. 7. Our neutrino analysis shows that for the NL3 EoS there is a drop of $\sim 2\text{--}3$ MeV in the average neutrino energy emitted from the merger remnants when the mass ratio goes from $q = 1$ to $q = 0.85$. For the DD2 EoS, no significant change or trend is seen in the neutrino average energies for these three particular snapshots.

The impact of the mass ratio on the neutrino emission properties of the post merger evolution appears to be stronger for the SFHo EoS simulations. Recall the observation in the temperature and Y_e distributions (Figs. 9 and 8) of the ejected mass and bound mass from the previous section. For the soft SFHo EoS, when comparing the $q = 1$ to the $q = 0.85$ mass ratio simulation, we saw a transition from shock heated–or interaction–ejecta to tidal ejecta and overall lower temperatures. Our neutrino analysis suggests that this transition has a direct and significant impact on the neutrino quantities; we observe significantly lower average neutrino energies ($\sim 6\text{--}8$ MeV; see Table V) and consequently predict a lower rate of neutrino detection for close by mergers. This analysis would indicate that observations of a few systems with different values of q (extracted from gravitational wave measurements of the individual NS masses) could hint at properties of the underlying EoS (see e.g. [85]).

We caution however that these observation are drawn

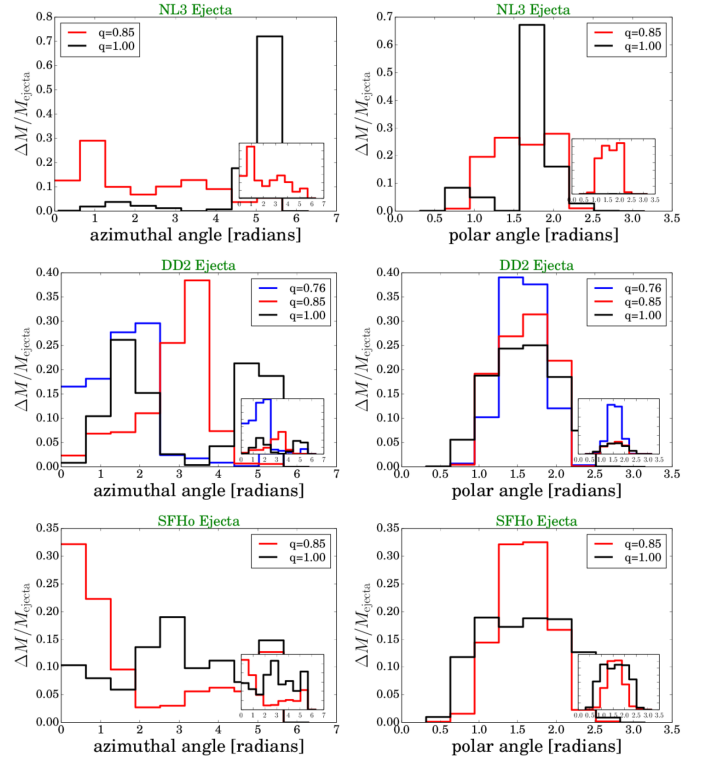


FIG. 11: *Azimuthal and polar angular distribution of unbound mass.* As in Figs. 8 and 9, the insets show the absolute quantities in arbitrary units.

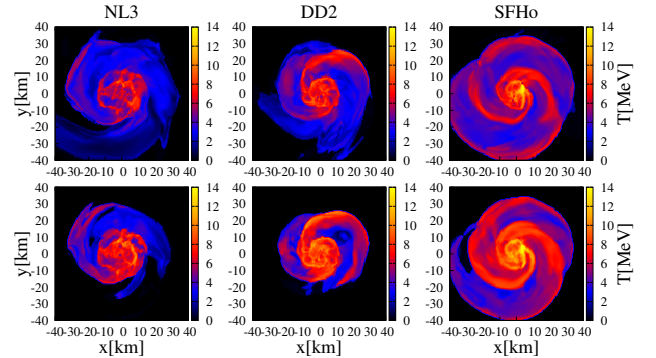


FIG. 12: *Electron neutrino (top) and electron antineutrino (bottom) surfaces as seen from the z -axis for the three different EoS considered in this work and a mass ratio $q = 0.85$, ~ 3 ms after the merger.*

from a detailed analysis at particular moments of time after merger in different simulations. These disks are highly perturbed and are undergoing rapid changes. It is important to explore this possibility more fully in the future by employing actual neutrino transport in order to obtain a better handle on the neutrino energy and

luminosity evolution as well as to capture the effects of neutrino absorption.

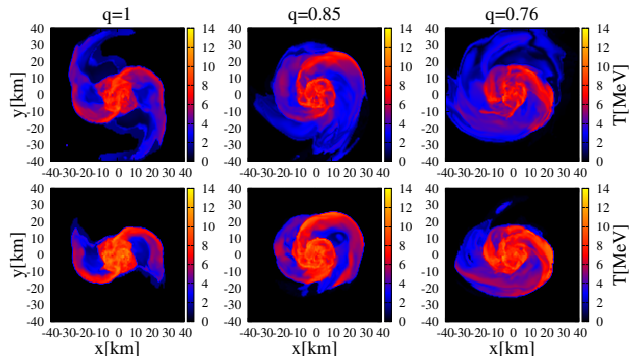


FIG. 13: Electron neutrino (top) and electron antineutrino (bottom) surfaces as seen from the z -axis for the DD2 EoS and different mass ratios q at $t = 3$ ms after the merger.

We end our discussion of the neutrino properties of the merger remnants by exploring the evolution of the neutrino luminosity. Fig. 14 shows the total neutrino luminosity as a function of time for all cases considered. Since neutrino production is strongly dependent on the temperatures achieved during and after the merger, a higher emission is expected as the EoS softens. Our simulations follow this trend (note the different scales in Fig. 14 for the different EoS).

As discussed throughout this paper, the merger yields a less violent collision for a given EoS as the mass ratio is decreased. This observation is also apparent in the neutrino luminosities. The equal mass cases show various episodes of higher neutrino luminosity (and neutrino average energy; see Table V) tied to the decompression stage that follows both the bounce (i.e. intensity maxima) and the occurrence of periods with higher relative intensity in gravitational waves. Our results suggest that unequal mass cases display a less oscillatory total neutrino luminosity. Although our sampling frequency of this luminosity is less than it was for the equal mass cases, we see no suggestions of the quite apparent oscillations of the $q=1$ cases. Furthermore, physically one would naturally expect that the oscillations would be more apparent in the symmetric, equal mass case as the bar-like remnant oscillated about a centrally condensed state. Once again, we stress the importance of a more detailed computation including neutrino transport to confirm the conclusions reached here.

The very rare observation of neutrinos from a close-by (galactic) neutron star merger would greatly complement the GW signature and reveal important information regarding the nuclear EoS. In combination with the electron antineutrino luminosities from our leakage scheme, we can use the average energies computed

EoS	q	t [ms]	$\langle E_{\bar{\nu}_e} \rangle$ [MeV]	$\langle E_{\nu_e} \rangle$ [MeV]	$L_{\bar{\nu}_e}$ [10^{53} erg/s]	R_ν [#/ms]
NL3	1.0	3.4	18.5 (22.4)	15.2 (18.3)	0.7	18
NL3	0.85	3.0	15.6 (18.7)	12.6 (15.1)	0.8	18
DD2	1.0	3.3	18.3 (22.1)	14.6 (17.4)	1.1	28
DD2	0.85	2.8	18.1 (21.7)	15.1 (18.0)	1.0	25
DD2	0.76	2.4	19.7 (23.9)	14.8 (17.9)	1.3	36
SFHo	1.0	3.5	24.6 (29.7)	23.5 (28.3)	3.5	121
SFHo	0.85	3.9	17.8 (21.3)	15.3 (17.9)	2.0	50

TABLE V: Neutrino properties at ~ 3 ms after the BNS merger for each EoS and mass ratio studied. The average energies $\langle E_{\bar{\nu}_e} \rangle$ and $\langle E_{\nu_e} \rangle$ are computed with (without) the gravitational redshift from our ray-tracing scheme while the electron antineutrino luminosity for the corresponding time is predicted from the leakage scheme. Also included is the estimated instantaneous detection rate in a SuperKamiokande-like water Cherenkov detector for a merger at 10 kpc from Earth, Eq. 13. The times are given with respect to t_{merger} , which is defined for each EoS as the time when the $q = 1$ mass ratio binary reaches first contact.

from our ray-tracing to estimate detection rates in a SuperKamiokande-like water-Cherenkov detector. These numbers are summarized in Table V. In addition to the three $q = 0.85$ mass ratio simulations, we also include in the table the results from the $q = 1$ simulations (with all three EoS) and the $q = 0.76$ simulation performed with the DD2 EoS. We note that the change in definition of merger time between this work and that of [25] causes slight differences in the value of t for the $q = 1$ snapshots [90]. To estimate the neutrino detection rates presented in Table V, we have made use of the following approximation

$$R_\nu \sim \frac{21.05}{\text{ms}} \left[\frac{M_{\text{water}}}{32 \text{ kT}} \right] \left[\frac{L_{\bar{\nu}_e}}{10^{53} \text{ erg/s}} \right] \left[\frac{\langle E_{\bar{\nu}_e} \rangle}{15 \text{ MeV}} \right] \left[\frac{10 \text{ kpc}}{D} \right]^2, \quad (13)$$

where $L_{\bar{\nu}_e}$ and $\langle E_{\bar{\nu}_e} \rangle$ are the electron antineutrino luminosity and average energy as listed in Table V. The details of this expression and the tracing technique are discussed in [25]. Our calculations suggest that discriminating the mass ratio based on neutrino detection alone is unlikely. However such a detection, especially if coincident or correlated with GWs, could shed light on the dynamics of stellar material near, and soon after, the point of merger.

IV. CONCLUSIONS

This work furthers our studies of the rich phenomenology of binary mergers, concentrating on unequal mass neutron star binaries with realistic equations of state and neutrino cooling. We focused on gravitational wave characteristics, ejecta and neutrino emission from the system and, in particular, identified features that can help ex-

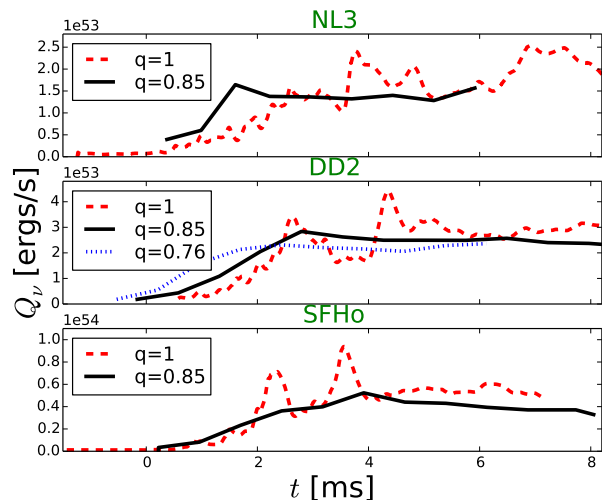


FIG. 14: Total neutrino luminosity from the BNS merger for the different mass ratios for each EoS. Shown are the NL3 EoS (top), DD2 EoS (middle), and SFHo (bottom). Note that the vertical scales differ in the three plots, with NL3 having the smallest range and SFHo the largest. Recall that mergers of unequal masses ($q < 1$) occur early, by up to ~ 1 ms for the NL3 and DD2 EoS.

tract the nuclear EoS from observations. As discussed, this information is encoded in observable signatures of gravity waves, electromagnetic radiation, and neutrinos, but extracting this information with a detection in only one of these channels might prove quite difficult. However, now that we have entered the era of GW detections, the possibility of collecting multiple merger events in different bands offers the promise of a deep understanding of the dynamics and EoS of these BNS systems.

Recent studies of BNS mergers have shown that the dominant frequencies of the post-merger GW signals reveal details of the EoS. However, the region of highest sensitivity for current GW detectors does not extend up to these merger frequencies, which limits our ability to extract EoS characteristics due to tidal effects. Before merger, tidal effects only become significant at the close separations achieved just before merger, and, again, these frequencies are generally higher than the most sensitive bandwidth of GW detectors.

We have found that the peak frequency in the gravitational waveform can be estimated via a fit based on a straightforward contact-frequency criteria which, in turn, relates directly to the EoS by the stellar radii. If the merger results in a kilonova, the resulting electromagnetic counterpart encodes more information about the

nuclear EoS. We studied the potential for equal mass binaries to produce a kilonova in recent work [25] finding the necessary conditions only for the softest EoS studied. However, as the mass ratio q decreases, we find that all three EoS considered produce significant ejecta with high neutron richness capable of producing a kilonova that peaks in the infrared (due to the production of heavy elements $A > 120$). For maximum effect therefore, electromagnetic observations of kilonovae afterglows from BNS need to be combined with gravitational wave measurements of the individual stellar masses. Neutrinos are also produced copiously by the merger and their energies appear to depend more strongly with the mass ratio for softer EoS, though further studies are required to confirm and quantify this possibility. Provided the merger occurs close enough to detect any neutrinos, their observation will provide valuable information on the EoS and complement the gravitational wave signature.

With the recent opening of the gravitational wave window, observing compact binary mergers through gravitational waves has become a reality. The combination of this new information with that enabled by electromagnetic signals and astroparticles will enable a deep understanding of such systems.

Acknowledgments

It is a pleasure to thank William East, Francois Foucart, Jonas Lippuner and Eric Poisson for interesting discussions as well as our collaborators Eric Hirschmann, Patrick Motl, and Marcelo Ponce. This work was supported by the NSF under grants PHY-1308621 (LIU), PHY-0969811 & PHY-1308727 (BYU), NASA’s ATP program through grant NNX13AH01G, NSERC through a Discovery Grant (to LL) and CIFAR (to LL). CP acknowledges support from the Spanish Ministry of Education and Science through a Ramon y Cajal grant and from the Spanish Ministry of Economy and Competitiveness grant FPA2013-41042-P. Additional support for this work was provided by NASA through Hubble Fellowship grant #51344.001-A (EO) awarded by the Space Telescope Science Institute, which is operated by the Association of Universities for Research in Astronomy, Inc., for NASA, under contract NAS 5-26555. Research at Perimeter Institute is supported through Industry Canada and by the Province of Ontario through the Ministry of Research & Innovation. Computations were performed at XSEDE and Scinet.

[1] **Virgo, LIGO Scientific** Collaboration, B. . Abbott *et al.*, “Observation of Gravitational Waves from a Binary Black Hole Merger,” *Phys. Rev. Lett.* **116** no. 6,

(2016) 061102, [arXiv:1602.03837](https://arxiv.org/abs/1602.03837) [gr-qc].
 [2] V. Connaughton *et al.*, “Fermi GBM Observations of LIGO Gravitational Wave event GW150914,”

- arXiv:1602.03920 [astro-ph.HE].
- [3] **Swift** Collaboration, P. A. Evans *et al.*, “Swift follow-up of the Gravitational Wave source GW150914,” arXiv:1602.03868 [astro-ph.HE].
- [4] **Fermi-LAT** Collaboration, “Fermi-LAT Observations of the LIGO event GW150914,” arXiv:1602.04488 [astro-ph.HE].
- [5] **Virgo, LIGO Scientific** Collaboration, B. P. Abbott *et al.*, “Tests of general relativity with GW150914,” arXiv:1602.03841 [gr-qc].
- [6] D. Blas, M. M. Ivanov, I. Sawicki, and S. Sibiriyakov, “On constraining the speed of gravitational waves following GW150914,” arXiv:1602.04188 [gr-qc].
- [7] J. Ellis, N. E. Mavromatos, and D. V. Nanopoulos, “Comments on Graviton Propagation in Light of GW150914,” arXiv:1602.04764 [gr-qc].
- [8] **Virgo, LIGO Scientific** Collaboration, B. P. Abbott *et al.*, “Astrophysical Implications of the Binary Black-Hole Merger GW150914,” *Astrophys. J.* **818** no. 2, (2016) L22, arXiv:1602.03846 [astro-ph.HE].
- [9] **Virgo, LIGO Scientific** Collaboration, B. P. Abbott *et al.*, “The Rate of Binary Black Hole Mergers Inferred from Advanced LIGO Observations Surrounding GW150914,” arXiv:1602.03842 [astro-ph.HE].
- [10] I. Mandel and S. E. de Mink, “Merging binary black holes formed through chemically homogeneous evolution in short-period stellar binaries,” arXiv:1601.00007 [astro-ph.HE].
- [11] P. Marchant, N. Langer, P. Podsiadlowski, T. Tauris, and T. Moriya, “A new route towards merging massive black holes,” arXiv:1601.03718 [astro-ph.SR].
- [12] A. Loeb, “Electromagnetic Counterparts to Black Hole Mergers Detected by LIGO,” arXiv:1602.04735 [astro-ph.HE].
- [13] R. Perna, D. Lazzati, and B. Giacomazzo, “Short Gamma-Ray Bursts from the Merger of Two Black Holes,” arXiv:1602.05140 [astro-ph.HE].
- [14] C. Palenzuela, L. Lehner, M. Ponce, S. L. Liebling, M. Anderson, D. Neilsen, and P. Motl, “Electromagnetic and Gravitational Outputs from Binary-Neutron-Star Coalescence,” *Phys. Rev. Lett.* **111** no. 6, (2013) 061105, arXiv:1301.7074 [gr-qc].
- [15] C. Palenzuela, L. Lehner, S. L. Liebling, M. Ponce, M. Anderson, *et al.*, “Linking electromagnetic and gravitational radiation in coalescing binary neutron stars,” *Phys.Rev.* **D88** no. 4, (2013) 043011, arXiv:1307.7372 [gr-qc].
- [16] M. Ponce, C. Palenzuela, L. Lehner, and S. L. Liebling, “Interaction of misaligned magnetospheres in the coalescence of binary neutron stars,” *Phys.Rev.* **D90** no. 4, (2014) 044007, arXiv:1404.0692 [gr-qc].
- [17] L. Lehner, C. Palenzuela, S. L. Liebling, C. Thompson, and C. Hanna, “Intense Electromagnetic Outbursts from Collapsing Hypermassive Neutron Stars,” *Phys.Rev.* **D86** (2012) 104035, arXiv:1112.2622 [astro-ph.HE].
- [18] N. R. Tanvir, A. J. Levan, A. S. Fruchter, J. Hjorth, R. A. Hounsell, K. Wiersema, and R. L. Tunnicliffe, “A ‘kilonova’ associated with the short-duration γ -ray burst GRB 130603B,” *Nature* **500** (Aug., 2013) 547–549, arXiv:1306.4971 [astro-ph.HE].
- [19] E. Berger, W. Fong, and R. Chornock, “An r-process Kilonova Associated with the Short-hard GRB 130603B,” *Astrophys.J.* **774** (2013) L23, arXiv:1306.3960 [astro-ph.HE].
- [20] E. Barausse, C. Palenzuela, M. Ponce, and L. Lehner, “Neutron-star mergers in scalar-tensor theories of gravity,” *Phys.Rev.* **D87** (2013) 081506, arXiv:1212.5053 [gr-qc].
- [21] C. Palenzuela, E. Barausse, M. Ponce, and L. Lehner, “Dynamical scalarization of neutron stars in scalar-tensor gravity theories,” arXiv:1310.4481 [gr-qc].
- [22] M. Shibata, K. Taniguchi, H. Okawa, and A. Buonanno, “Coalescence of binary neutron stars in a scalar-tensor theory of gravity,” arXiv:1310.0627 [gr-qc].
- [23] L. Sampson, N. Yunes, N. Cornish, M. Ponce, E. Barausse, A. Klein, C. Palenzuela, and L. Lehner, “Projected Constraints on Scalarization with Gravitational Waves from Neutron Star Binaries,” *Phys. Rev.* **D90** no. 12, (2014) 124091, arXiv:1407.7038 [gr-qc].
- [24] M. Ponce, C. Palenzuela, E. Barausse, and L. Lehner, “Electromagnetic outflows in a class of scalar-tensor theories: Binary neutron star coalescence,” *Phys. Rev.* **D91** no. 8, (2015) 084038, arXiv:1410.0638 [gr-qc].
- [25] C. Palenzuela, S. L. Liebling, D. Neilsen, L. Lehner, O. L. Caballero, E. O’Connor, and M. Anderson, “Effects of the microphysical equation of state in the mergers of magnetized neutron stars with neutrino cooling,” *Phys. Rev. D* **92** no. 4, (Aug., 2015) 044045, arXiv:1505.01607 [gr-qc].
- [26] D. Neilsen, S. L. Liebling, M. Anderson, L. Lehner, E. O’Connor, *et al.*, “Magnetized Neutron Stars With Realistic Equations of State and Neutrino Cooling,” *Phys.Rev.* **D89** no. 10, (2014) 104029, arXiv:1403.3680 [gr-qc].
- [27] J. M. Lattimer, “The nuclear equation of state and neutron star masses,” *Annual Review of Nuclear and Particle Science* **62** no. 1, (2012) 485–515, <http://dx.doi.org/10.1146/annurev-nucl-102711-095018>, <http://dx.doi.org/10.1146/annurev-nucl-102711-095018>.
- [28] A. W. Steiner, M. Hempel, and T. Fischer, “Core-collapse Supernova Equations of State Based on Neutron Star Observations,” *ApJ* **774** (Sept., 2013) 17, arXiv:1207.2184 [astro-ph.SR].
- [29] M. Hempel, T. Fischer, J. Schaffner-Bielich, and M. Liebendörfer, “New Equations of State in Simulations of Core-collapse Supernovae,” *ApJ* **748** (Mar., 2012) 70, arXiv:1108.0848 [astro-ph.HE].
- [30] P. Demorest, T. Pennucci, S. Ransom, M. Roberts, and J. Hessels, “Shapiro Delay Measurement of A Two Solar Mass Neutron Star,” *Nature* **467** (2010) 1081–1083, arXiv:1010.5788 [astro-ph.HE].
- [31] J. Antoniadis, P. C. Freire, N. Wex, T. M. Tauris, R. S. Lynch, *et al.*, “A Massive Pulsar in a Compact Relativistic Binary,” *Science* **340** (2013) 6131, arXiv:1304.6875 [astro-ph.HE].
- [32] LORENE. home page <http://www.lorene.obspm.fr/>, 2010.
- [33] E. Poisson and C. M. Will, *Gravity*. May, 2014.
- [34] J. Vines, E. E. Flanagan, and T. Hinderer, “Post-1-Newtonian tidal effects in the gravitational waveform from binary inspirals,” *Phys.Rev.* **D83** (2011) 084051, arXiv:1101.1673 [gr-qc].
- [35] T. Mora and C. M. Will, “A PostNewtonian diagnostic of quasidequilibrium binary configurations of compact

- objects,” *Phys. Rev.* **D69** (2004) 104021, [arXiv:gr-qc/0312082](#) [gr-qc]. [Erratum: *Phys. Rev.* **D71**, 129901(2005)].
- [36] T. Damour and A. Nagar, “Effective one body description of tidal effects in inspiralling compact binaries,” *Phys. Rev. D* **81** no. 8, (Apr., 2010) 084016, [arXiv:0911.5041](#) [gr-qc].
- [37] T. Dietrich, S. Bernuzzi, M. Ujevic, and B. Brügmann, “Numerical relativity simulations of neutron star merger remnants using conservative mesh refinement,” *Phys. Rev. D* **91** no. 12, (June, 2015) 124041, [arXiv:1504.01266](#) [gr-qc].
- [38] T. Hinderer, “Tidal Love numbers of neutron stars,” *Astrophys. J.* **677** (2008) 1216–1220, [arXiv:0711.2420](#) [astro-ph].
- [39] W. E. East, V. Paschalidis, F. Pretorius, and S. L. Shapiro, “Relativistic Simulations of Eccentric Binary Neutron Star Mergers: One-arm Spiral Instability and Effects of Neutron Star Spin,” *Phys. Rev.* **D93** no. 2, (2016) 024011, [arXiv:1511.01093](#) [astro-ph.HE].
- [40] S. Chawla *et al.*, “Mergers of Magnetized Neutron Stars with Spinning Black Holes: Disruption, Accretion and Fallback,” *Phys. Rev. Lett.* **105** (2010) 111101, [arXiv:1006.2839](#) [gr-qc].
- [41] K. D. Kokkotas and B. G. Schmidt, “Quasi-normal modes of stars and black holes,” *Living Reviews in Relativity* **2** no. 2, (1999) . <http://www.livingreviews.org/lrr-1999-2>.
- [42] A. Bauswein and N. Stergioulas, “A unified picture of the post-merger dynamics and gravitational wave emission in neutron-star mergers,” *ArXiv e-prints* (Feb., 2015) , [arXiv:1502.03176](#) [astro-ph.SR].
- [43] W. Kastaun and F. Galeazzi, “Properties of hypermassive neutron stars formed in mergers of spinning binaries,” *Phys. Rev. D* **91** no. 6, (Mar., 2015) 064027, [arXiv:1411.7975](#) [gr-qc].
- [44] K. Takami, L. Rezzolla, and L. Baiotti, “Spectral properties of the post-merger gravitational-wave signal from binary neutron stars,” *Phys. Rev. D* **91** no. 6, (Mar., 2015) 064001, [arXiv:1412.3240](#) [gr-qc].
- [45] F. Foucart, R. Haas, M. D. Duez, E. O’Connor, C. D. Ott, L. Roberts, L. E. Kidder, J. Lippuner, H. P. Pfeiffer, and M. A. Scheel, “Low mass binary neutron star mergers : gravitational waves and neutrino emission,” [arXiv:1510.06398](#) [astro-ph.HE].
- [46] R. De Pietri, A. Feo, F. Maione, and F. Löffler, “Modeling Equal and Unequal Mass Binary Neutron Star Mergers Using Public Codes,” *ArXiv e-prints* (Sept., 2015) , [arXiv:1509.08804](#) [gr-qc].
- [47] S. Bernuzzi, T. Dietrich, and A. Nagar, “Modeling the Complete Gravitational Wave Spectrum of Neutron Star Mergers,” *Physical Review Letters* **115** no. 9, (Aug., 2015) 091101, [arXiv:1504.01764](#) [gr-qc].
- [48] T. Dietrich, N. Moldenhauer, N. K. Johnson-McDaniel, S. Bernuzzi, C. M. Markakis, B. Bruegmann, and W. Tichy, “Binary Neutron Stars with Generic Spin, Eccentricity, Mass ratio, and Compactness - Quasi-equilibrium Sequences and First Evolutions,” *ArXiv e-prints* (July, 2015) , [arXiv:1507.07100](#) [gr-qc].
- [49] T. Damour, A. Nagar, and L. Villain, “Measurability of the tidal polarizability of neutron stars in late-inspiral gravitational-wave signals,” *Phys.Rev.* **D85** (2012) 123007, [arXiv:1203.4352](#) [gr-qc].
- [50] J. Lattimer and D. Swesty *Nucl. Phys. A* **535** (1991) 331–376.
- [51] N. Tacik *et al.*, “Binary Neutron Stars with Arbitrary Spins in Numerical Relativity,” *Phys. Rev.* **D92** no. 12, (2015) 124012, [arXiv:1508.06986](#) [gr-qc].
- [52] S. Bernuzzi, A. Nagar, T. Dietrich, and T. Damour, “Modeling the Dynamics of Tidally Interacting Binary Neutron Stars up to the Merger,” *Phys.Rev.Lett.* **114** no. 16, (2015) 161103, [arXiv:1412.4553](#) [gr-qc].
- [53] K. Hotokezaka, K. Kyutoku, and M. Shibata, “Exploring tidal effects of coalescing binary neutron stars in numerical relativity,” *Phys.Rev.* **D87** no. 4, (2013) 044001, [arXiv:1301.3555](#) [gr-qc].
- [54] T. Hinderer *et al.*, “Effects of neutron-star dynamic tides on gravitational waveforms within the effective-one-body approach,” [arXiv:1602.00599](#) [gr-qc].
- [55] J. S. Read, L. Baiotti, J. D. E. Creighton, J. L. Friedman, B. Giacomazzo, *et al.*, “Matter effects on binary neutron star waveforms,” *Phys.Rev.* **D88** (2013) 044042, [arXiv:1306.4065](#) [gr-qc].
- [56] B. J. Owen, “Search templates for gravitational waves from inspiraling binaries: Choice of template spacing,” *Phys.Rev.* **D53** (1996) 6749–6761, [arXiv:gr-qc/9511032](#) [gr-qc].
- [57] T. Baumgarte, P. Brady, J. D. E. Creighton, L. Lehner, F. Pretorius, *et al.*, “Learning about compact binary merger: The Interplay between numerical relativity and gravitational-wave astronomy,” *Phys.Rev.* **D77** (2008) 084009, [arXiv:gr-qc/0612100](#) [gr-qc].
- [58] J. S. Read, C. Markakis, M. Shibata, K. Uryu, J. D. Creighton, *et al.*, “Measuring the neutron star equation of state with gravitational wave observations,” *Phys.Rev.* **D79** (2009) 124033, [arXiv:0901.3258](#) [gr-qc].
- [59] “Ligo document t0900288-v3.” <https://dcc.ligo.org/cgi-bin/DocDB/ShowDocument?docid=2974>.
- [60] B. D. Lackey and L. Wade, “Reconstructing the neutron-star equation of state with gravitational-wave detectors from a realistic population of inspiralling binary neutron stars,” *Phys. Rev.* **D91** no. 4, (2015) 043002, [arXiv:1410.8866](#) [gr-qc].
- [61] M. Agathos, J. Meidam, W. Del Pozzo, T. G. F. Li, M. Tompitak, J. Veitch, S. Vitale, and C. V. D. Broeck, “Constraining the neutron star equation of state with gravitational wave signals from coalescing binary neutron stars,” *Phys. Rev.* **D92** no. 2, (2015) 023012, [arXiv:1503.05405](#) [gr-qc].
- [62] J. S. Bloom, D. E. Holz, S. A. Hughes, K. Menou, A. Adams, *et al.*, “Astro2010 Decadal Survey Whitepaper: Coordinated Science in the Gravitational and Electromagnetic Skies,” [arXiv:0902.1527](#) [astro-ph.CO].
- [63] **LIGO Scientific Collaboration, Virgo Collaboration** Collaboration, M. Branchesi, A. Klotz, and M. Laas-Bourez, “Searching for electromagnetic counterparts of gravitational wave transients,” [arXiv:1110.3169](#) [astro-ph.IM].
- [64] N. Andersson, J. Baker, K. Belczynski, S. Bernuzzi, E. Berti, *et al.*, “The Transient Gravitational-Wave Sky,” *Class.Quant.Grav.* **30** (2013) 193002, [arXiv:1305.0816](#) [gr-qc].
- [65] B. D. Metzger and E. Berger, “What is the Most Promising Electromagnetic Counterpart of a Neutron

- Star Binary Merger?," *ApJ* **746** (Feb., 2012) 48, [arXiv:1108.6056 \[astro-ph.HE\]](#).
- [66] D. Radice, F. Galeazzi, J. Lippuner, L. F. Roberts, C. D. Ott, and L. Rezzolla, "Dynamical Mass Ejection from Binary Neutron Star Mergers," [arXiv:1601.02426 \[astro-ph.HE\]](#).
- [67] L.-X. Li and B. Paczynski, "Transient events from neutron star mergers," *Astrophys.J.* **507** (1998) L59, [arXiv:astro-ph/9807272 \[astro-ph\]](#).
- [68] S. Kulkarni, "Modeling supernova-like explosions associated with gamma-ray bursts with short durations," [arXiv:astro-ph/0510256 \[astro-ph\]](#).
- [69] B. D. Metzger, G. Martínez-Pinedo, S. Darbha, E. Quataert, A. Arcones, D. Kasen, R. Thomas, P. Nugent, I. V. Panov, and N. T. Zinner, "Electromagnetic counterparts of compact object mergers powered by the radioactive decay of r-process nuclei," *MNRAS* **406** (Aug., 2010) 2650–2662, [arXiv:1001.5029 \[astro-ph.HE\]](#).
- [70] K. Hotokezaka, K. Kyutoku, M. Tanaka, K. Kiuchi, Y. Sekiguchi, *et al.*, "Progenitor models of the electromagnetic transient associated with the short GRB 130603B," [arXiv:1310.1623 \[astro-ph.HE\]](#).
- [71] T. Piran, O. Korobkin, and S. Rosswog, "Implications of GRB 130603B and its macronova for r-process nucleosynthesis," [arXiv:1401.2166 \[astro-ph.HE\]](#).
- [72] D. Kasen, R. Fernández, and B. Metzger, "Kilonova Light Curves from the Disk Wind Outflows of Compact Object Mergers," [arXiv:1411.3726 \[astro-ph.HE\]](#).
- [73] R. Fernández, D. Kasen, B. D. Metzger, and E. Quataert, "Outflows from accretion discs formed in neutron star mergers: effect of black hole spin," *Mon.Not.Roy.Astron.Soc.* **446** (2015) 750–758, [arXiv:1409.4426 \[astro-ph.HE\]](#).
- [74] R. Fernández, E. Quataert, J. Schwab, D. Kasen, and S. Rosswog, "The interplay of disk wind and dynamical ejecta in the aftermath of neutron star - black hole mergers," [arXiv:1412.5588 \[astro-ph.HE\]](#).
- [75] K. Hotokezaka, K. Kiuchi, K. Kyutoku, H. Okawa, Y.-i. Sekiguchi, M. Shibata, and K. Taniguchi, "Mass ejection from the merger of binary neutron stars," *Phys. Rev. D* **87** no. 2, (Jan., 2013) 024001, [arXiv:1212.0905 \[astro-ph.HE\]](#).
- [76] J. M. Lattimer and D. N. Schramm, "Black-hole-neutron-star collisions," *ApJ* **192** (Sept., 1974) L145–L147.
- [77] D. M. Meyer, D. E. Welty, and D. G. York, "Element abundances at high redshift," *ApJ* **343** (Aug., 1989) L37–L40.
- [78] D. Eichler, M. Livio, T. Piran, and D. N. Schramm, "Nucleosynthesis, neutrino bursts and gamma-rays from coalescing neutron stars," *Nature* **340** (July, 1989) 126–128.
- [79] J. Barnes and D. Kasen, "Effect of a High Opacity on the Light Curves of Radioactively Powered Transients from Compact Object Mergers," *Astrophys.J.* **775** (2013) 18, [arXiv:1303.5787 \[astro-ph.HE\]](#).
- [80] E. Nakar and T. Piran, "Radio Remnants of Compact Binary Mergers - the Electromagnetic Signal that will follow the Gravitational Waves," *Nature* **478** (2011) 82–84, [arXiv:1102.1020 \[astro-ph.HE\]](#).
- [81] M. H. Ruffert, H. T. Janka, and G. Schaefer, "Coalescing neutron stars: A step towards physical models. I: Hydrodynamic evolution and gravitational-wave emission," *Astron. Astrophys.* **311** (1996) 532–566, [arXiv:astro-ph/9509006](#).
- [82] S. Rosswog and M. Liebendoerfer, "High resolution calculations of merging neutron stars. 2: Neutrino emission," *Mon.Not.Roy.Astron.Soc.* **342** (2003) 673, [arXiv:astro-ph/0302301 \[astro-ph\]](#).
- [83] E. O'Connor and C. D. Ott, "A New Open-Source Code for Spherically-Symmetric Stellar Collapse to Neutron Stars and Black Holes," *Class.Quant.Grav.* **27** (2010) 114103, [arXiv:0912.2393 \[astro-ph.HE\]](#).
- [84] O. L. Caballero, G. C. McLaughlin, and R. Surman, "Detecting neutrinos from black hole-neutron star mergers," *Phys. Rev. D* **80** no. 12, (Dec., 2009) 123004, [arXiv:0910.1385 \[astro-ph.HE\]](#).
- [85] C. M. Will, "The confrontation between general relativity and experiment," *Living Reviews in Relativity* **9** no. 3, (2006) . <http://www.livingreviews.org/lrr-2006-3>.
- [86] K. Hotokezaka, K. Kyutoku, H. Okawa, M. Shibata, and K. Kiuchi, "Binary Neutron Star Mergers: Dependence on the Nuclear Equation of State," *Phys.Rev.* **D83** (2011) 124008, [arXiv:1105.4370 \[astro-ph.HE\]](#).
- [87] We adopt the convention $m_2 \geq m_1$ so that $q \leq 1$.
- [88] Remnants with total mass not significantly larger than the maximum allowed mass for a rotating neutron star for a given EOS can avoid prompt collapse, e.g [86].
- [89] As a certain amount of compression results in the collision, the true gravitational frequency is naturally higher.
- [90] In Ref. [25], the merger time used for the neutrino calculations measured time with respect to a merger time calculated via the peak GW amplitude instead of the time of first contact.